

# NUMERICAL INVESTIGATION OF THE TURBULENT FLOW PARAMETERS DISTRIBUTION IN A PARTLY PERFORATED HORIZONTAL WELLBORE

*Mohammed Abdulwahhab Abdulwahid*

Research Scholar, Department of Marine Engineering,  
Andhra University, AP, India

*Ass. Prof. Sadoun Fahad Dakhil*

Department of Fuel& Energy, Basrah Technical College, Iraq

*Prof. Niranjan Kumar Injeti*

Department of Marine Engineering, Andhra University, AP, India

---

## Abstract

The overall pressure drop in a horizontal wellbore used in the recovery of oil and gas industry was classified into four separate effects due to wall friction, increase in momentum, perforation roughness and type of fluid mixing. A perforated section is followed by a plain section for many horizontal wells. The additional pressure drop due to combined effect of perforation roughness and the type of fluid mixing was analyzed through numerical CFD and the results were compared with the experimental results of other researchers. The computations were based on the finite volume method with the SIMPLE algorithm standard  $k - \varepsilon$  model. The pipe was used geometrically similar to the real perforated wellbore with  $60^\circ$  phasing, 6 SPF (shoot per foot) and the pitch of the perforations 60 mm (the number of perforations in this paper are less than experimental pipe). The parameters that are being investigated are pressure drops of the pipe and so far simulations have been carried out for an inlet pipe Reynolds numbers ranging from 28,773 to 90,153 for the total flow rate ratio ranging from 0% to 100%. Numerical simulations were performed using CFX of ANSYS FLUENT 13, where the governing equations of mass and momentum were solved simultaneously, using the two equations of standard  $k - \varepsilon$  turbulence model. As the rate of flow through the perforations increases i.e. with the increase in flow rate ratio, the total pressure increases due to large acceleration pressure drop for higher flow rate through the perforations. The increases in perforations number increase the total pressure drop and vice versa. The numerical results agreed with the experimental work.

---

**Keywords:** Pressure drop, perforation, wellbore, Reynolds number, numerical, total flow rate ratio

## **1: Introduction.**

Over the last decade horizontal wells have become a well-established technology for the recovery of oil and gas. Considerable amount of analytical and experimental work has been published on various aspects of horizontal well used in the production which includes transient flow models, productivity indices, and cresting behavior. Although these methods provide insight into the behavior of horizontal wells, certain methods have considered the pressure drop along the wellbore and essentially assuming infinite conductivity. The pressure drop in the pipe can severely limit the actual production length of the pipe. It is clear from the above that frictional effects will lead to a significant drop in the pressure between the heel and the toe of the well.

An accurate set of single-phase experiments in a perforated pipe with radial inflow has been conducted by (Su and Gudmundsson, 1995) (SG). SG conducted the experiment to account for the total pressure drop in a perforated pipe is contributed by frictional, accelerational pressure drops and pressure drop due to the effects of radial inflow and mixing pressure drop. SG observed that the frictional and accelerational pressure drops are significant parts of the total pressure drop. However, the mixing pressure drop is significant and its contribution to the pressure drop is often negative. Additionally, when the velocities of the radial and axial are equal, the radial flow will penetrate the axial pipe and blockage of the pipe. This will lead to an increase of the pressure drop in the pipe.

Ouyang et al., (1996) performed experiments to determine the friction factors for pipe flow with radial inflow in laminar and turbulent flow. The friction factor based on the Stanford horizontal wellbore data yields a friction factor in which the correlation due to radial inflow is dependent on the Reynolds number of the flow in the radial perforation. Ouyang et al., (1996) also mentioned that for turbulent flow, inflow reduces the wall friction.

Ouyang et al., (1998) studied a single-phase wellbore flow model that incorporated not only frictional, accelerational, and gravitational pressure drop, but also the pressure drop caused by inflow. The new model was readily applicable to different wellbore-perforation patterns and well completions, and was easily incorporated into reservoir simulators or analytical, reservoir-inflow models. It was found that the influence of either inflow or outflow depended on the flow regime present in the wellbore. It was found that the accelerational pressure drop may or may not be important compared to the frictional component, depending on the specific pipe

geometry, fluid properties and flow conditions. It was recommended that the new wellbore-flow model be included in wellbore/reservoir coupling models to achieve more accurate predictions of pressure drop and inflow distribution along the wellbore, as well as the well production or injection rates.

Kloster, (1990) experiment studied flow resistance in a perforated pipe, both with and without flow injection. The Reynolds numbers covered from 45,000 to 60,000. The friction factor values were 25-70% higher than those of regular commercial pipes. He also observed that small injections through perforations reduced the friction factor. A new friction factor correlation for horizontal wellbore was proposed by (Asheim *et al.*, 1992) which included accelerational pressure losses due to continuous fluid influx along the wellbore. They assumed that the injected fluid entered the main flow with no momentum in the axial direction. Ihara *et al.*, (1994) performed experiments that studied the channel flow with continuous influx into the horizontal wellbore from the oil reservoir. The pressure drop along the test channel increased due to the effect of influx. The model of one-dimension momentum exchange agreed with the experimental data for relatively large Reynolds numbers.

The friction factor of perforation roughness was measured in pipes geometrically on par with casing used in horizontal wells. There was no fluid flow through the perforations in the work reported. The experimental data was analyzed using the universal velocity distribution law and the concept of roughness function. It was found that the roughness function increased linearly with the perforation/casing diameter ratio. An empirical relationship was obtained to estimate the friction factor in pipes with perforation roughness (Su and Gudmundsson, 1998).

The aim of this work is to demonstrate the alternate use of CFD simulations instead of experiments to estimate the pressure drops, the pressure drop coefficients at the horizontal wellbore and the effect of the perforation density for a range of locally changing flow ratios and Reynolds numbers. The total pressure drop incorporates not only frictional, accelerational pressure drops but also the pressure caused by inflow. The main difference between the theoretical study in this paper with the experiments carried out by SG are the diameter of perforations and the perforation density of the pipe. SG has used a perforation diameter of 3mm and 158 perforations, where as in this present study, a perforation of 4mm diameter and 60 perforations has been used.

The paper is organized as follows. The authors start with some theoretical background of the work. This is followed by details of the geometry and numerical model and discussion of the relevant parameters which influence the pressure loss. Subsequently, numerical results are presented and a detailed data analysis is carried out.

## 2: Theoretical Analysis.

### 2.1. Model Description.

The physical model description is that of a partly perforated pipe and a plain pipe without perforation. The length of the pipe is equal to 1300 mm and 22 mm diameter as shown in figure 1. The pipe is divided into two sections with equal length. The perforated section is part of the pipe that has a 600 mm, perforation phasing  $60^\circ$  and Simulation Perforation Density 6 (SPF). The pitch of the perforations is 60 mm with a perforation diameter of 4 mm. The other section, 600 mm in length is divided into four equal sections of 150 mm. Each one to investigate the pressure profile along the pipe when there is a perforated section upstream. Pipe and perforation geometry for experimental and theoretical study is listed in Table 2.1.

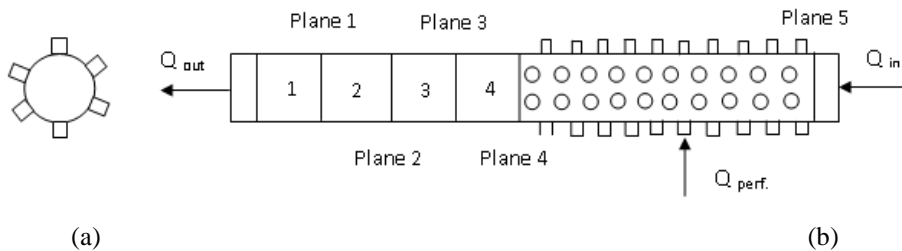


Figure (1) Configuration of partly perforated test pipe (not to scale).

The computational domain having same dimensions is to be considered as experimental rigs (Su and Gudmundsson, 1998). The geometry has been analysed using 3 dimensional Computational Fluid Dynamics (CFD). Figure 2 is the unstructured computational grid, the mesh consist of 169574 nodes and 666177 elements with five boundary layers. The calculations carried out were with commercial finite volume code ANSYS FLUENT 13 CFX5 using a first order scheme and a turbulent with k epsilon model.

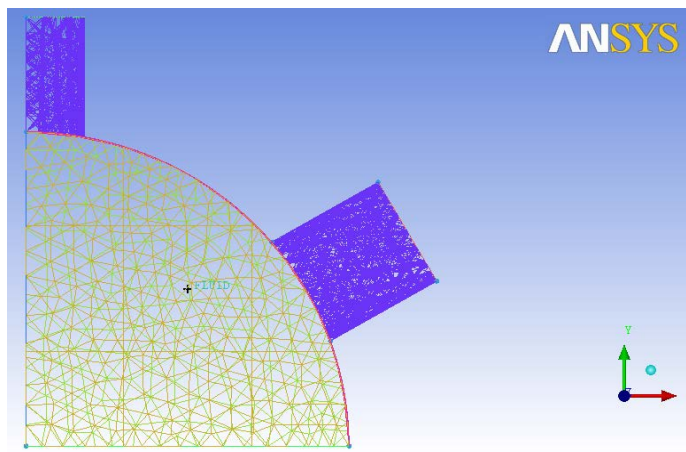


Figure (2) The unstructured mesh for partly perforated pipe.

**Table 2.1. Geometry of the test pipe.**

Item	Experimental	Theoretical
Outer Diameter	30 mm	-
Inner Diameter	21.94 mm	22 mm
Perfo. Diameter	3.0 mm	4.0 mm
Total perfo. number	158	60
Perfo. phasing	60 °	60 °
Perfo. density	12 SPF	6 SPF

## 2. 2. Simulation Parameters.

The fluid considered for the simulations is water with constant density of 998.2 kg/m<sup>3</sup> and dynamic viscosity of 0.001 kg/m s. The fluid is assumed as Incompressible flow. Three tests were carried out with Reynolds number of the inlet flow ranging from 28,773 to 90,153. In each of the tests, the flow rate through the perforations was increased from zero to maximum value. The roughness of the test pipe wall was 0.03 mm; the type of the test pipe was PVC. Test details are summarized in table 2.2.

Table 2.2 Parameters of partly perforated pipe tests.

Test	Inlet Flow Rate (liter/hr)	Perforation inlet Flow Rate (liter/hr)	Inlet Flow (Re)
Test 1	5,157-5,618	0-841	82,756-90,153
Test 2	3,361-3,836	0-854	53,935-61,557
Test 3	1,793-2,318	0-899	28,773-37,198

Uniform water mass flow is introduced at the inlet of a partially perforated pipe. Two boundary conditions are considered. At the inlet, mass flow rate is taken into consideration both axially and radially where as at the exit, outlet pressure is considered as the boundary condition. It is assumed that no-slip boundary conditions occur along the walls. Water enters at a uniform temperature (T) of 25° C. For the symmetry lines both velocity and pressure is kept constant.

## 3. Theoretical Simulations.

Over a long period of time the pressure drop in a fully developed turbulent pipe flow is being studied by several researchers and investigators. The pressure drop in a straight pipe has been determined in numerous experiments. In this study, the general model developed by (Su and Gudmundsson, 1998) was adopted to analyze the acquired data. They suggested pressure terms like acceleration, friction, perforation roughness and fluid mixing pressure drop components. The following relationship gives the four pressure drop terms that make up the total pressure drop in a perforated horizontal well

$$\Delta p = \Delta p_{acc.} + \Delta p_{wall} + \Delta p_{perfo.} + \Delta p_{mix.} \quad (1)$$

The pressure drop caused by perforation roughness and fluid mixing were lumped together and classified as additional losses. Eq. 1 can then be rewritten as

$$\Delta p = \Delta p_{acc.} + \Delta p_{wall} + \Delta p_{add}. \tag{2}$$

Applying the conservation of linear momentum to the control volume in the axial direction for each perforation unit within equal length  $\Delta L$ , results in the sum of the forces acting on the control volume surfaces towards the downstream direction of the pipe axis

$$\sum F = m'_{out}u_{out} - m'_{in}u_{in} \tag{3}$$

where the mass flow rate is

$$m' = \rho Au \tag{4}$$

When radial inflow occurs, the static pressure in the pipe is not uniform, and the velocity profile is not fully developed. In addition to the force contributed by the pressure difference across the control volume and wall shear force, the sum of the forces acting on the control volume surface includes a force due to the combined effects of the irreversible process of fluid mixing and the presence of the perforation hole, including the effect of non-uniformly distribution of static pressure and non-fully developed velocity profile,

$$\sum F = (p_{in}A - p_{out}A) - \tau_w(\pi D \Delta L) - F_{add}. \tag{5}$$

From the above equations, this can be rearranged to get the following total pressure drop,

$$p_{in} - p_{out} = \rho(u_{out}^2 - u_{in}^2) + \Delta p_{wall} + \Delta p_{add}. \tag{6}$$

Eq. (6) indicates that the total pressure drop consists of three different components:

- The pressure drop due to kinematic energy change (acceleration effects). This demonstrates the first term on the right side of Eq. (6).
- The frictional pressure drop due to wall friction in a perforation unit,  $\Delta p_{wall}$ , the second term of Eq. (6), and can be calculated from the Darcy-Wesibach equation (White, 1986),

$$\Delta p_{wall} = \frac{f}{2} \frac{\Delta L}{D} \rho v^2 \tag{7}$$

When the relative roughness of the pipe is known, an accurate and convenient relationship for the friction factor in the turbulent pipe flow is the Haaland equation (Haaland, 1983)

$$f = \left\{ -1.8 \log_{10} \left[ \frac{6.9}{Re} + \left( \frac{\varepsilon}{3.7D} \right)^{1.11} \right] \right\}^{-2} \tag{8}$$

For a hydraulically smooth pipe, surface roughness  $\varepsilon$  should be set to zero.

This equation applies to both laminar and turbulent flow.

- The additional losses pressure drop term was obtained from the measured pressure drop after subtracting the pressure drop contribution due to wall friction and fluid acceleration.

The pressure drop due to mixing effects arises from the interaction between perforation flow and wellbore flow which is causing disturbances in the boundary layer and hence affects the pressure drop. The fluid enters radially to the wellbore through a perforation. It mixes with the axial flow and increases mass into the well, thereby increasing the flow velocity in the well. Hence, the acceleration of the flow will increase the velocity at the outer. This gives a pressure drop across the perforation. Subtracting the accelerational and frictional pressure drops from the total pressure drop that flows through the perforations, the remaining pressure drop is a practical representation of the additional pressure drop  $\Delta P_{add}$  (perforation roughness and mixing effects).

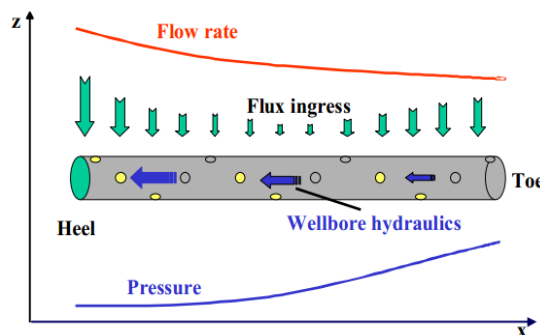


Figure (3) Horizontal completion effect on reservoir influx and wellbore hydraulic (Yula, 2001).

Figure 3 illustrates the interplay between the pressure and flux distribution along the wellbore through the completion openings. It shows the increase in flow rate from toe to heel but the decrease in pressure from toe to the heel.

#### 4. Results and Discussions.

##### 4.1. Total Pressure Drop in Perforated section.

Theoretically was carried out on the pipe that was simulated with the experimental pipe. Three tests with different pipe flow rates for axial flow and radial flow were carried out and the results are shown in table 2.1. Figure 4 represents the total pressure drop in the perforated section with total flow rate ratio where  $q = \text{total perforation flow rate divided by the total flow rate}$

at the pipe outlet for the three tests. The total pressure drop values are calculated using equation 1 and 2. It is observed that there is an increase in flow rate ratio as the rate flow through perforation increases. The total pressure drop increased due to the larger acceleration pressure drop at higher flow rate through the perforations. The total pressure drop was found to be higher for higher Reynolds numbers. For higher axial flow velocity there is larger frictional pressure drop at the wall. The increase of radial flow through perforations increases the total flow rate ratio and increases the total pressure drop. The total pressure drop of 60 perforations (for the present paper) is lesser than the total pressure drop of 158 perforations (experimental pipe). This is because the perforation density of the experimental pipe is twice and a half larger than that of the pipe for the present paper.

The total pressure drop according to Eq. 2 is equal to the acceleration, frictional pressure drops and the effect of fluid mixing and perforation roughness. The total flow rate ratio increased due to the increase in the flow through the perforations that increased the total pressure drop. This is due to the larger acceleration pressure drop for higher flow rate through the perforations.

Figure 5 depicts the total pressure drop in the entire pipe which is similar to the behavior as shown in figure 4. The values of total pressure drop for the entire pipe is higher than the total pressure drop in the perforated section for all the tests. For test 1, the values of the total pressure drop in the whole pipe is larger than the values in the perforated section in the range of 34.2% to 25.5% at 0% to 100% flow rate ratio respectively, for test 2, within the range of 33.9% to 22% and for test 3 within the range of 35.3% to 19.4%. The increase of the total pressure drop in the whole pipe is due to the wall friction pressure drop in the plain section.

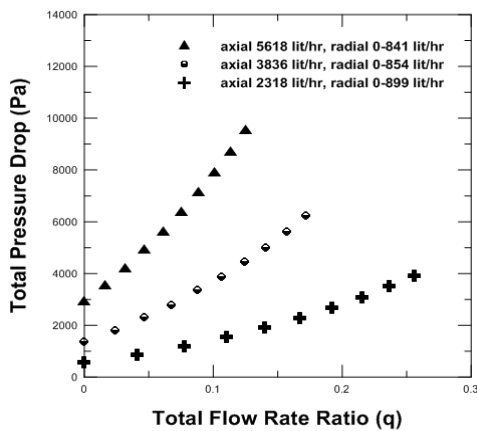


Figure (4) Total pressure drop in perforated section, with different tests condition.

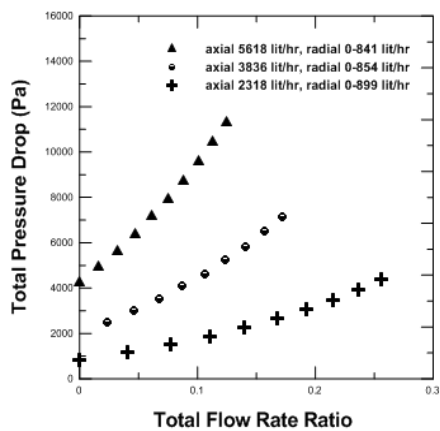


Figure (5) Total Pressure drop in the whole pipe with different tests condition.

#### 4.2. Pressure Drop in Perforated Section.

Three tests with different pipe flow rates were carried out on the perforated pipe. The pressure drop due to momentum change (acceleration pressure drop) was calculated from Eq. 6 (the first term on the right side). It is noticed that the values of acceleration pressure drop for partly perforated wellbore were high. The pressure drop due to momentum increased for each test. The inlet mean velocity at the inlet of the perforated section and the outlet mean velocity at the outlet of the perforated section, the velocities and the pressure drop due to momentum were calculated. Figure 6 represents the relationship between pressure drop due to momentum and total flow rate ratio ( $q$ ). It depicts that the increase in the pressure drop with increase in the value of  $q$  for all tests is similar to the behavior in figure 4.

Figure 7 represents the behavior of additional pressure drop for the three tests. The additional pressure drop decreases as the flow rate ratio increases. In the present numerical analysis all the values of the additional pressure drop are negative. When the perforation inflow increases the total pressure decreases and the frictional pressure drop decreases too. The values of additional pressure drop are negative. Figure 7 illustrates the frictional pressure drop that was reduced when the flow rate ratio was increased.

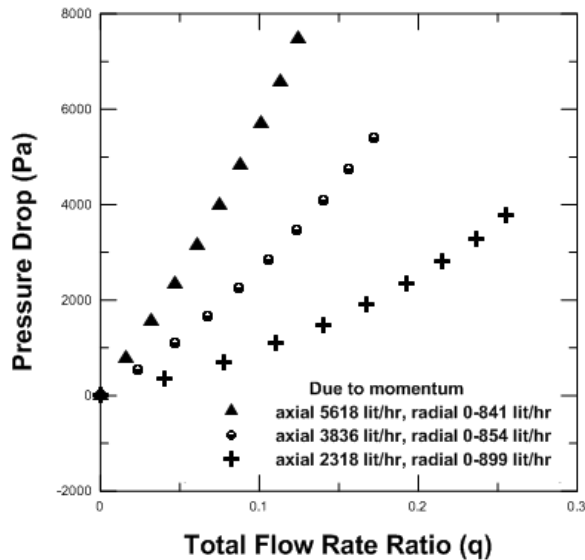


Figure (6) Pressure drop with effect of momentum forces in perforated section.

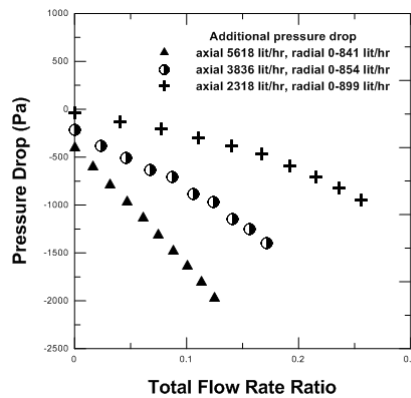


Figure (7) Additional pressure drop for different tests.

The pressure drop increases with the increase of Reynolds numbers which contributes to the larger wall friction pressure drop with higher flow velocities. The ordinary wall friction pressure drop of a perforated section was calculated using the Darcy-Weisbach equation.

For the turbulent flow, the axial velocity gradient near the pipe wall decreases and hence the wall friction shear stress also decreases accordingly. On the contrary, outflow lowers and reduces the boundary layer and thus decreases the average velocity outside the layer but increases the velocity inside the layer, which results in an increase of the axial velocity gradient near the pipe wall and hence the wall friction shear stress (Ouyang et al., 1997).

### 4.3. Pressure Drop Coefficient.

Pressure drop in a perforated section is the function of the flow rate in the pipe. Therefore, the numerical results from different tests are interested in the pressure drop coefficient parameter. A pressure drop coefficient represents an important parameter which is defined as the pressure drop across the perforated section divided by the kinetic energy at the outlet of the pipe.

$$k = \frac{\Delta P}{0.5 * \rho * U^2} \tag{9}$$

where  $U$  is the average flow velocity at the outlet of the test pipe.

The pressure drop coefficients were calculated for total and additional pressure drops for perforated section and for the whole pipe for all the three tests. The data points for each test follow a straight line as shown in figure 8. Data points of the three tests for total pressure drop followed parallelly and closely for some points of those tests conducted with Reynolds number range from 82,756 to 90,153 and from 53,935 to 61,557. The pressure drop coefficients increase linearly with increasing total flow rate ratio.

Figure 9 represents the pressure drop coefficient in the whole pipe i.e. perforation section as well as plain section. In figure 11 there is a drastic change in the values between the three tests. The values of pressure drop coefficient for test 3 (axial 1793 lit/hr and radial from 0 to 899 lit/hr) are much higher compared to test 1 and 2. This is because the value of axial velocity is less than the other tests.

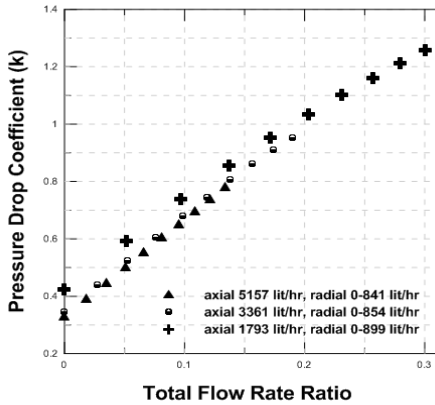


Figure (8) Pressure drop coefficient in perforated section, with different tests condition.

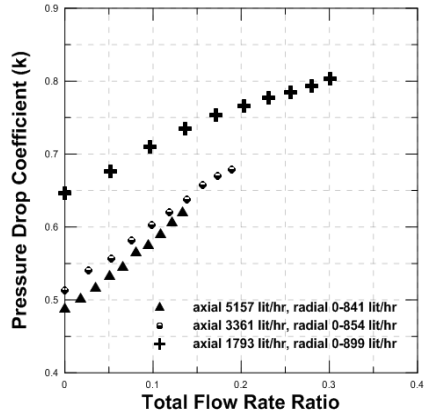


Figure (9) Pressure drop coefficient in the whole pipe, with different tests condition.

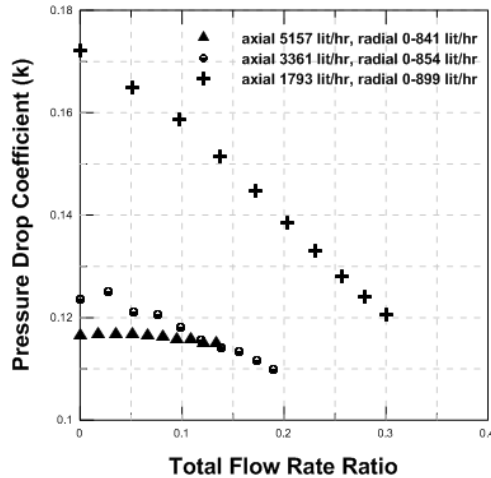


Figure (10) Pressure drop coefficient in plain section, with different tests condition.

Figure 10 represents the results of pressure drop coefficient in the plain section for the three tests. The pressure drop coefficient decreases with the increase in total flow rate ratio. The pressure drop coefficient for test 3 is higher than the values of the other tests. This is due to lower values of axial velocity at the entry of the plain section of the pipe; the pressure drop coefficient is high. On the contrary, with the higher values of the axial velocity, there is a drop in the values of the pressure drop coefficient.

Figure 11 represents the velocity distribution contour for axial flow rate of 5618 lit/hr and radial flow of 841 lit/hr in the perforated section. The flow velocity increases due to the mixing of the axial flow with radial flow at the junction. It is noticed that there is a drop in pressure and rise in flow rate at the perforated section.

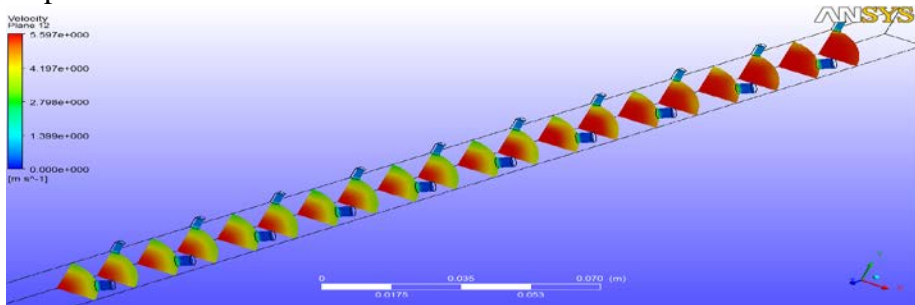
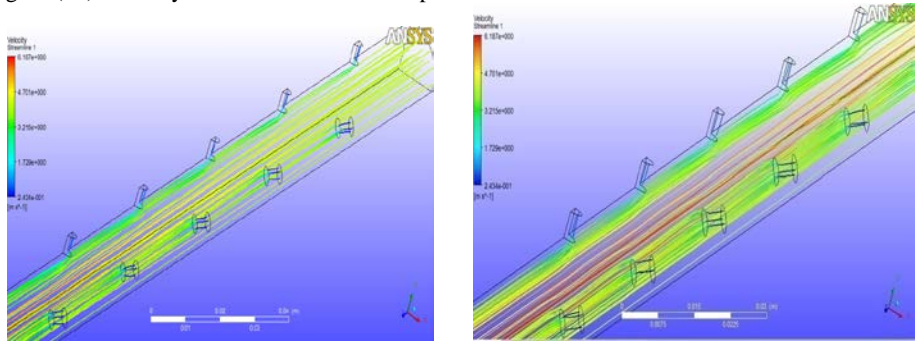


Figure (11) Velocity distribution contour for perforated section axial 5618 lit/hr & radial 841 lit/hr.



(a) At first perforations.

(b) At last perforations.

Figure (12) Velocity streamlines for perforated section, axial 5618 lit/hr & radial 841 lit/hr.

Figure 12 illustrates velocity streamlines for perforated section when the axial flow is 5618 lit/hr and the radial flow is 841 lit/hr. It is observed that there is a rise in axial velocity at the end of the perforated section due to flow through perforations.

#### 4.4. Turbulence Intensity.

The turbulent intensity  $Ti$  is linked to the kinetic energy and a reference mean flow velocity as follows:

$$Ti = \frac{\left(\frac{2}{3}k\right)^{0.5}}{U} \quad (10)$$

The equations to be solved for incompressible flow are the conservation of mass Eq. (11) and momentum Eq. (12) in Cartesian coordinate.

$$\frac{\partial U_i}{\partial x_i} = 0 \quad (11)$$

$$\frac{\partial \rho U_i}{\partial t} + \frac{\partial \rho U_j U_i}{\partial x_j} = -\frac{\partial \bar{p}}{\partial x_i} + \frac{\partial}{\partial x_j} \left[ \mu \left( \frac{\partial U_i}{\partial x_j} + \frac{\partial U_j}{\partial x_i} \right) - \overline{\partial \rho u_i u_j} \right] \quad (12)$$

where: u is main axial velocity and U is bulk velocity.

The Transport equations for  $k - \varepsilon$  model are for  $k$ ,

$$\frac{\partial}{\partial t} (\rho k) + \frac{\partial}{\partial x_i} (\rho k u_i) = \frac{\partial}{\partial x_j} \left[ \left( \mu + \frac{\mu_t}{\sigma_k} \right) \frac{\partial k}{\partial x_j} \right] + p_k + p_b - \rho \varepsilon - Y_k + S_k \quad (13)$$

And For  $\varepsilon$ ,

$$\frac{\partial}{\partial t} (\rho \varepsilon) + \frac{\partial}{\partial x_i} (\rho \varepsilon u_i) = \frac{\partial}{\partial x_j} \left[ \left( \mu + \frac{\mu_t}{\sigma_\varepsilon} \right) \frac{\partial \varepsilon}{\partial x_j} \right] + C_{1\varepsilon} \frac{\varepsilon}{k} (P_k + C_{3\varepsilon} P_b) - C_{2\varepsilon} \rho \frac{\varepsilon^2}{k} + S_\varepsilon \quad (14)$$

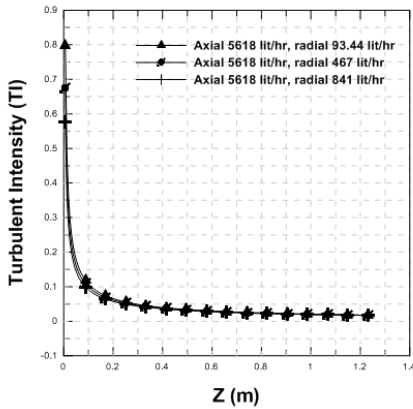


Figure (13) Turbulent Intensity for 5618 lit/hr with different radial values.

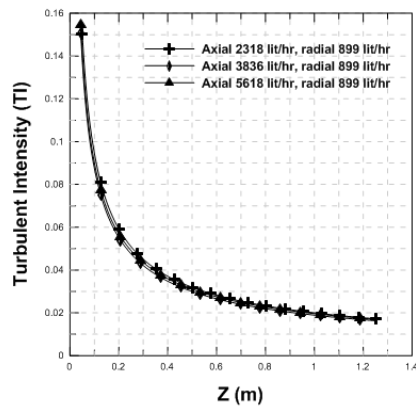


Figure (14) Turbulent Intensity for different Axial flows with radial 899 lit/hr.

Figure 13 represents turbulent intensity for a fixed axial flow of 5618 lit/hr with different radial flow values of 93.44, 467 and 841 lit/hr. As a consequence, using an optimized power curve fit is the best fit for every individual case over the new upper and lower limits. It has a higher value of turbulent intensity at the inlet of the wellbore for all the three tests, and lower value of turbulent intensity in the flow along the wellbore.

Figure 14 represents turbulent intensity for a fixed radial flow of 899 lit/hr with different axial flow values of 2318, 3836, and 5618 lit/hr. Power curve fit was applied, and resultant curves were shown and compared with the curves from figure 15. The curves for varying axial flows with fixed radial flow show that there is a sharp drop in turbulent intensity.

Figure 15 shows the comparison between the numerical simulations (present work) with experimental work (Su and Gudmundsson, 1998). It is observed that the graphs drawn for the experimental work and the numerical simulations are appearing to have similar behavior but the values are

different between the three tests. The percentage error for test 2 with ranging from 42.44% at zero of the total flow rate ratio and decreasing to 1.4% at 0.100785 for total flow rate ratio and then the values of total pressure drop of the present work increasing so that the percentage error increases from 4.4% to 7.4%. The percentage error for test 2 with ranging from 42.39% at zero of the total flow rate ratio and decreasing to 3.1% at 0.106173 for total flow rate ratio and then, the values of total pressure drop of present work increasing so that the percentage error increases from 5.9% to 16.5%. Finally, for test 3 ranging from 42.24% at zero of the total flow rate ratio and decreasing to 14.4% at 0.11027 for total flow rate ratio and then the values of total pressure drop of the present work increasing so that the percentage error increases from 2.8% to 33.8%. The total pressure drop values of the experimental work were obviously larger than those of present work. After a certain value of the total flow rate ratio, the values of the total pressure drop increased. This was because the perforation density of experimental work [9] was twice and a half larger than of the present work.

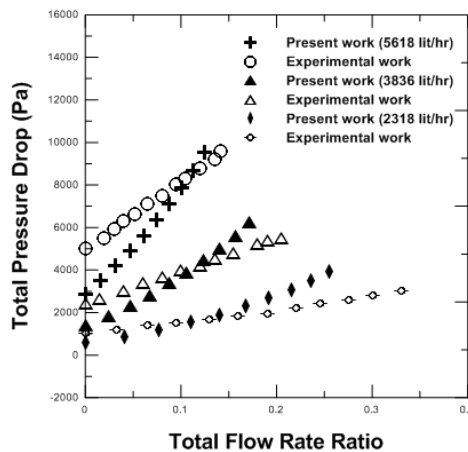


Figure (15) Comparison of numerical simulation and experimental data (Su and Gudmundsson, 1998).

## 5. Conclusion

Numerical simulations have been carried out on the flow in a partly perforated pipe with inflow through the perforations. The geometry of the pipe that was used approximately similar to the pipe used in the experiment (Su and Gudmundsson, 1998), except the pitch of the perforations was 30 mm with a perforation diameter of 4 mm and perforation density of 6 (SPF) instead of a perforation diameter of 3 mm and 12 (SPE) as adopted in the experimental test rig.

- 1- The total pressure drop in the perforated section of the pipe increased with increase in the flow rate ratio, but the value of the total pressure drop in the whole pipe was greater than the value in the perforated section.

- 2- A large amount of numerical data was acquired. The Reynolds numbers were in the range approximately from 28,000 to 90,000.
- 3- The additional pressure drop decreases as the flow rate ratio increased. The additional pressure drop was of a negative value after 0.04 of total flow rate ratio ( $q$ ) which resulted from a total pressure drop, but the additional pressure drop resulting from the pressure drop was still of a positive value with increase in the total flow rate ratio.
- 4- The axial velocity increased at the end of the perforated section due to flow through perforations.
- 5- The values of the total pressure drop in the whole pipe were larger than the values in the perforated section.
- 6- The total pressure drop values of the experimental work were obviously larger than those of the present work due to the difference in perforation density.
- 7- Numerical results have demonstrated that the number of perforations have relationship with increase or decrease in the total pressure drop. The increases in perforations number are increased in the total pressure drop and vice versa.
- 8- The numerical results agreed with the experimental work (Su and Gudmundsson, 1998).

### Acknowledgements

To all the people who helped me, thank you. Thank you for my special appreciation to Prof. T.V.K. Bhanuprakash for providing numerous answers to my countless questions.

### Nomenclature

$C_{1\epsilon}$	Standard k-epsilon model constant [-]	$u_i$	velocity (fluct. ith comp.) [m/s]
$C_{2\epsilon}$	Standard k-epsilon model constant [-]	$u_1$	average axial velocity at inlet [m/s]
$C_k$	Standard k-epsilon model constant [-]	$u_2$	average axial velocity at outlet [m/s]
$D$	pipe inner diameter [m]	$U$	bulk velocity [m/s]
$f$	friction factor [-]	$\Delta L$	length between perforations [m]
$k$	turbulent kinetic energy [ $m^2/s^2$ ]	$\Delta P$	total pressure drop [Pa]
$P_b$	effect of buoyancy [-]	$\Delta P_{acc.}$	pressure drop due to momentum [Pa]
$P_k$	production of k [-]	$\Delta P_{add}$	additional pressure drop [Pa]
$S$	modulus of the mean rate of strain tensor [-]	$\Delta P_{perfo}$	Press. drop due to perforation roughness
$t$	time [s]	$\Delta P_{mixing}$	pressure drop due to fluid mixing [Pa]

